The Company of Biologists

SHORT REPORT

High-speed multifocal plane fluorescence microscopy for three-dimensional visualisation of beating flagella

Benjamin J. Walker[1] and Richard J. Wheeler[2,*]

ABSTRACT

Analysis of flagellum and cilium beating in three dimensions (3D) is important for understanding cell motility, and using fluorescence microscopy to do so would be extremely powerful. Here, high-speed multifocal plane fluorescence microscopy, where the light path is split to visualise multiple focal planes simultaneously, was used to reconstruct *Trypanosoma brucei* and *Leishmania mexicana* movement in 3D. These species are uniflagellate unicellular parasites for which motility is vital. It was possible to use either a fluorescent stain or a genetically-encoded fluorescent protein to visualise flagellum and cell movement at 200 Hz frame rates. This addressed two open questions regarding *Trypanosoma* and *Leishmania* flagellum beating, which contributes to their swimming behaviours: 1) how planar is the *L. mexicana* flagellum beat, and 2) what is the nature of flagellum beating during *T. brucei* 'tumbling'? We showed that *L. mexicana* has notable deviations from a planar flagellum beat, and that during tumbling the *T. brucei* flagellum bends the cell and beats only in the distal portion to achieve cell reorientation. This demonstrates high-speed multifocal plane fluorescence microscopy as a powerful tool for the analysis of beating flagella.

KEY WORDS: Cilia, Flagella, *Leishmania*, Microscopy, *Trypanosoma*

INTRODUCTION

Trypoanosomatid parasites, including the human pathogens *Trypanosoma brucei*, *Trypanosoma cruzi* and *Leishmania* spp., have a single flagellum whose motility is vital for progression through the life cycle (Beneke et al., 2019; Broadhead et al., 2006; Rotureau et al., 2013; Shimogawa et al., 2018). Different species and life cycle stages have linked morphological and motility adaptations, and trypanosomatid morphologies are defined, in part, by the flagellum that is laterally attached to the cell body along most of its length in the trypomastigote morphology, for a shorter portion of its length in the epimastigote and simply protrudes from the cell anterior in the promastigote (Hoare and Wallace, 1966) (Fig. 1A).

Trypanosoma brucei trypomastigotes, including procyclic (fly midgut) and mammalian bloodstream forms, have a complex three-dimensional (3D) cell movement (Bargul et al., 2016; Heddergott et al., 2012; Rodríguez et al., 2009; Schuster et al., 2017; Wheeler, 2017). They can swim in liquid, but the fly gut and salivary glands

can be densely packed with parasite cells (Schuster et al., 2017). When they are free in a volume of liquid, such as the bloodstream, they swim far slower than the fluid flow (Heddergott et al., 2012; Krüger et al., 2018), yet they can invade tissues (Capewell et al., 2016; Trindade et al., 2016). Taken together, this suggests complex motility functions, which includes collective motion of densely packed cells (Eliaz et al., 2017; Imhof and Roditi, 2015; Oberholzer et al., 2010; Saada et al., 2015) and surface-bound antibody clearance (Cheung et al., 2016; Engstler et al., 2007). *Leishmania* promastigote and *T. cruzi* epimastigote swimming is somewhat unlike *T. brucei* (Ballesteros-Rodea et al., 2012; Gadelha et al., 2007; Wheeler, 2017), and the function of their motility is less well-analysed but is probably also complex (Forestier et al., 2011). As for *T. brucei*, they will also probably undergo hydrodynamic coupling when densely packed, which could give collective population movement at the macro scale.

Contributing to complex motility are at least two modes of flagellum movement. *T. brucei*, *T. cruzi*, *Leishmania* and related organisms normally undergo a tip-to-base symmetrical flagellar-type beat (Holwill, 1965; Walker, 1961). In *Leishmania* promastigotes and *T. cruzi* epimastigotes this is near-planar (Gadelha et al., 2007; Holwill and McGregor, 1975; Wheeler, 2017) and at ∼20–25 Hz in *Leishmania* (Gadelha et al., 2007; Wheeler, 2017). They can also switch to a base-to-tip beat (Ballesteros-Rodea et al., 2012; Edwards et al., 2018; Gadelha et al., 2007; Heddergott et al., 2012; Holwill and McGregor, 1975). In *T. cruzi* epimastigotes and *Leishmania* promastigotes this reversed beat is an asymmetrical ciliary-type beat at lower frequency [6±1 Hz (mean±s.e.m.) in *L. major*] and causes cell reorientation (Ballesteros-Rodea et al., 2012; Edwards et al., 2018; Gadelha et al., 2007). The function of beat type-switching is not yet clear; however, persistent base-to-tip beating in *Leishmania* (upon deletion of the distal outer dynein arm docking complex protein dDC2; LmxM.31.2900) (Edwards et al., 2018) prevents transmission through the sandfly vector (Beneke et al., 2019). In *T. brucei* the tip-to-base beat occurs at ∼15–20 Hz (Branche et al., 2006; Heddergott et al., 2012; Rodríguez et al., 2009; Schuster et al., 2017; Wheeler, 2017). The reversed beat is not so well characterised [except in mutants (Baron et al., 2007; Branche et al., 2006)], but occurs at a lower frequency [∼3–5 Hz in procyclic forms (Branche et al., 2006), 13.1±0.8 in bloodstream forms (Heddergott et al., 2012)] with a higher amplitude. It causes slow backwards swimming or 'tumbling' (Heddergott et al., 2012), a term used to describe rapid cell reorientation. Again, switching to a reversed beat has no clear function, but different *T. brucei* life cycle stages in the tsetse fly vector have different propensities for tumbling (Schuster et al., 2017).

Previous analyses of trypanosomatid cell and/or flagellum movement have been two-dimensional, with three exceptions for *T. brucei*. One is qualitative, defocus of bright-field microscopy to infer distance from the focal plane (Heddergott et al., 2012). Two are quantitative, an optical tomography approach (Heddergott et al., 2012) and mathematical model fitting (Wheeler, 2017). However,

[1]Wolfson Centre for Mathematical Biology, Mathematical Institute, University of Oxford, Oxford OX2 6GG, UK. [2]Peter Medawar Building for Pathogen Research, Nuffield Department of Medicine, University of Oxford, Oxford OX1 3SY, UK.

*Author for correspondence (richard.wheeler@ndm.ox.ac.uk)

B.J.W., 0000-0003-0853-267X; R.J.W., 0000-0002-4270-8360
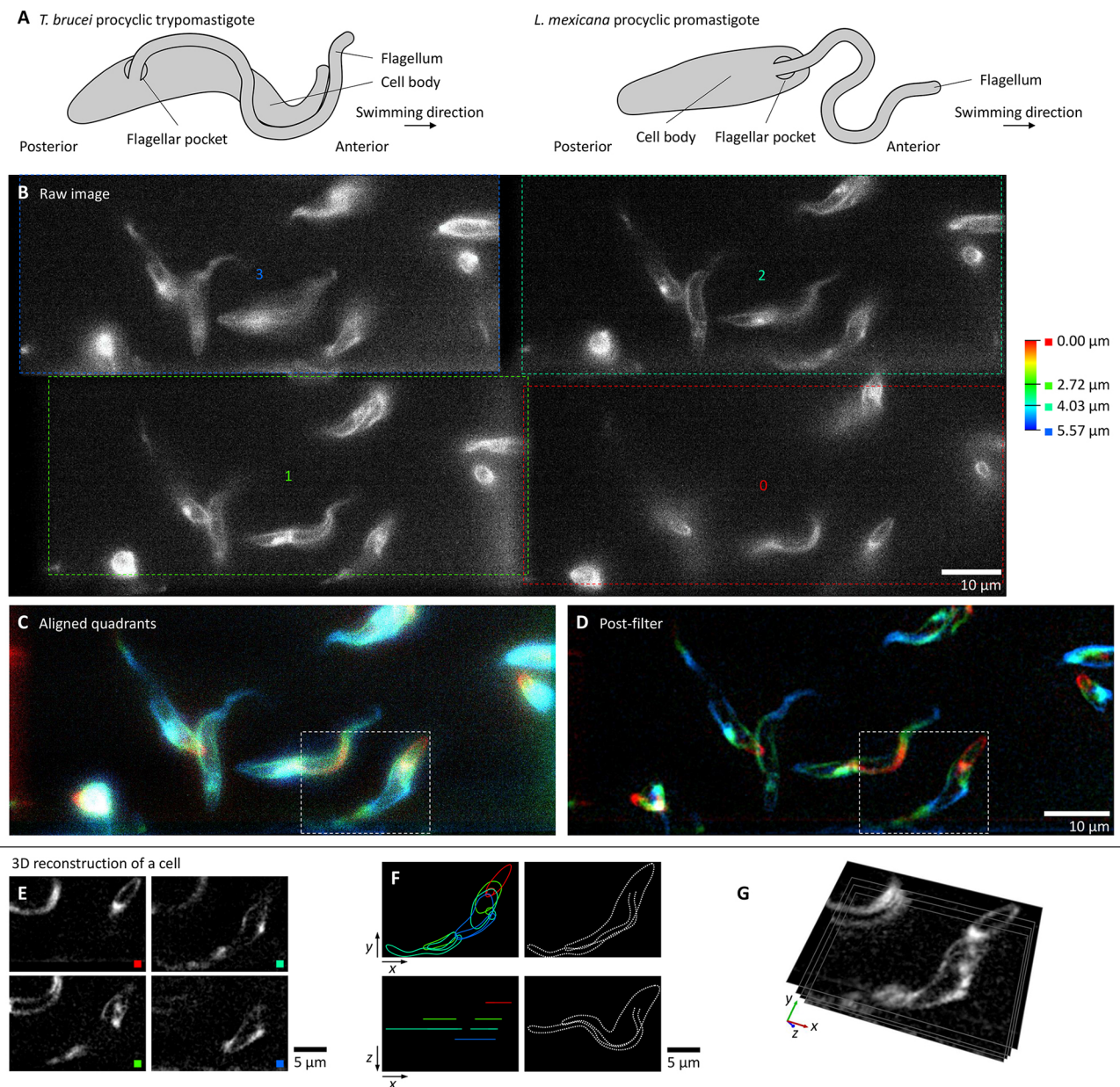
Fig. 1. High-speed multifocal plane microscopy to visualise live swimming *T. brucei* in 3D. All micrographs show a single frame from a 200 Hz video of procyclic forms labelled with FM 4-64FX (Movie 1). (A) Schematic representation of the morphology of *T. brucei* and *L. mexicana* procyclic forms. (B) The raw camera image, showing the four sub-images (0–3) and their focal offsets. (C) The image in B, following sub-image alignment and pseudocolouring according to focal depth. (D) The image in C following filtering. (E–G) 3D reconstruction of an example cell, outlined in white box in C and D, showing individual focal planes (E), membrane contours from each focal plane (left) and the 3D conformation (right) (F), and direct visualisation in 3D (G).

both quantitative methods required a perfectly repeating beat and constant cell rotation rate. More broadly, three main approaches have been used to perform 3D flagellar beat analysis. First, inferring defocus distance using bright-field microscopy (Bukatin et al., 2015), which is limited to semi-quantitative depth information. Second, using a high-frequency oscillating objective (rapid focus change) to visualise multiple focal planes (Silva-Villalobos et al., 2014). Here, focal planes capture is only near-synchronous, leading to a 3D analogue of rolling shutter artefacts. Objective motion will also give blurring in *z*. Third, high-speed digital holographic microscopy, as used for sperm (Daloglu et al., 2018) and *Plasmodium* microgametes (Wilson et al., 2013). This has relatively low signal-to-noise and requires complex image analysis. These approaches have only been used 'label free' using transmitted light illumination – indeed,

inferred defocus distance and digital holographic microscopy can only be used with transmitted light.

Multifocal plane fluorescence microscopy (Gan et al., 2013; Prabhat et al., 2007) has the potential to achieve the frame rates and sensitivities necessary for analysis of flagellum beating in 3D, with the advantage of high fluorescent label specificity. Here, it was applied to open questions concerning *T. brucei* and *L. mexicana* motility. First, using membrane stain FM 4-64FX to analyse *T. brucei* flagellum beating during tumbling, which has not previously been analysed in 3D. This showed that tumbling arises from reversed distal flagellum beating while the proximal flagellum 'locks' the cell in a curved configuration that may arise from proximal and/or distal differences in axoneme (particularly outer dynein arm) composition (Edwards et al., 2018; Subota et al., 2014).

Second, a fluorescent protein fused to a flagellar membrane protein at the endogenous locus was used to quantify *Leishmania* beat planarity, previously assumed to be near-planar. This showed that flagellum bending remains within a plane, but that the plane can change over a beat cycle. This requires twisting at the flagellum base, probably linked with flagellum attachment in the pocket (Wheeler et al., 2016) or factors specific to the proximal axoneme (Edwards et al., 2018). *Leishmania* have a tendency to swim in curved paths (Wheeler, 2017) and this phenomenon may be responsible.

RESULTS AND DISCUSSION

Multifocal plane imaging was initially tested with *T. brucei* labelled with FM 4-64FX in normal growth medium. *T. brucei* movement deviates significantly from a single plane and requires 100 Hz or faster frame rates to effectively 'freeze' flagellum/cell movement for analysis. Multifocal plane imaging was configured using a light path multi-splitter with three semi-silvered mirrors, which split the light to four quadrants of a single camera, and lenses at the pupil planes to introduce focus offsets (Fig. S1A). Lens focal lengths were selected for a ~2 μm focal plane (z) spacing and the actual focus offset and the sub-image position on the camera sensor (in x and y) were calibrated using fluorescent beads (Fig. S1). Sub-image image position and magnification aberration was measured and corrected (Fig. S1B,C,D), allowing precise sub-images alignment into a final z stack.

200 Hz frame rates were achieved with a 2560×1080 px image resolution. At four focal planes this corresponds to ~0.5 gigavoxel/ second with ~8 photons/px background and signal up to ~50 photons/px (Fig. 1B; Movie 1A). Sub-image alignment and colour coding by focal plane offset gives a 3D view of cell conformation (Fig. 1C; Movie 1B) and image filtering highlights the in-focus membrane at each focal plane (Fig. 1D; Movie 1C), effectively capturing *T. brucei* morphology (Fig. 1E). The cell and flagellum membrane contours can be interpreted to give a plausible 3D configuration, including the position of the flagellum and flagellar pocket at its base (Fig. 1F). Alternatively, the data can be directly visualised in 3D (Fig. 1G).

Flagellum beat during *T. brucei* tumbling

T. brucei 'tumbling' associated with beat reversal occurs commonly in the metacyclic forms in tsetse fly salivary glands (Schuster et al., 2017) and occasionally in other life cycle stages (Branche et al., 2006; Heddergott et al., 2012; Uppaluri et al., 2011). While it has no unambiguous function, understanding tumbling is valuable as it causes cell reorientation that could allow a 'run and tumble'-like chemotaxis mechanism. *T. brucei* experience a low Reynolds number environment where reversal of the flagellum beat for forward swimming would simply reverse swimming direction (Purcell, 1977). Therefore, tumbling must also involve some other change; perhaps an unrecognised asymmetry in the reversed *T. brucei* beat or perhaps, as previously noted (Heddergott et al., 2012), a difference in motion between the proximal and distal flagellum. Analysing tumbling cells is challenging as they have a 'less straight' configuration (Uppaluri et al., 2011) that sits poorly in a focal plane.

To characterise tumbling, procyclic form cells were labelled with FM 4-64FX and placed in a sample chamber. Tumbling cells sedimented near the coverslip and 200 Hz multifocal plane videos showed that they all underwent a reversed beat; however, in the majority (75%, n=28) the proximal half of the flagellum did not move. Instead, the waveforms initiated in the middle of the flagellum and propagated towards the tip (Fig. 2A; Movie 2A). In the remainder, the entire flagellum moved and the waveforms initiated near the flagellum base (Fig. 2B; Movie 2B). Tumbling was similar to the motion of outer dynein arm mutants following RNAi knockdown of intermediate (DNAI1) (Branche et al., 2006) or light (LC1) (Baron et al., 2007) chains. This further supports the hypothesis that beat reversal in *T. brucei* involves changes to outer dynein arm regulation.

Forward-swimming cells under the same conditions underwent a tip-to-base flagellum beat while rotating around their long axis (Fig. S2). This matches previous analysis by optical tomography (bloodstream forms) (Heddergott et al., 2012) and mathematical model fitting (procyclic forms) (Wheeler, 2017), and is incompatible with a bihelical beat (Rodríguez et al., 2009).

In tumbling cells where flagellum movement was restricted to the distal half of the flagellum (the cell anterior), the proximal half of the flagellum (the cell middle) was 'locked' in a curve on a ~100 ms timescale (Fig. 2A; Movie 2A). Viewing these cells in 3D (Fig. 2C) showed a ~90° bend in the middle of the cell that was not always clear from 2D images. The distal flagellum beat plane was perpendicular to the plane in which the proximal flagellum bent the cell, consistent with a helical attachment of the flagellum to the cell body. The impact of cell curvature on swimming was simulated using a boundary element computational framework, which showed a 90° mid-cell bend that causes a circular swimming path with a radius less than the cell length (Fig. S3), qualitatively similar to reorientation while tumbling. The flagellum in tumbling cells is therefore responsible for a beat and cell configuration that are not a time reversal of the normal tip-to-base beat, leading to rapid reorientation and explaining why tumbling cells appear less straight.

For forward swimming, waveforms initialise at the flagellum tip, while, for tumbling, flagellar waveforms tend to initialise mid-flagellum rather than at the flagellum base. Sites conducive for waveform initiation may be defined by proximal and/or distal differences in the molecular composition of outer dynein arms (Edwards et al., 2018) or other axoneme components (Subota et al., 2014). Alternatively, as cell body and flagellum movement are tightly coupled by the flagellum attachment zone and the attached cell body is wider towards the flagellum base, it may be too rigid (Sun et al., 2018) for the reversed beat to bend.

Procyclic *L. mexicana* beat planarity

Leishmania (and related species) have a near-planar flagellum beat but have only been analysed when confined to a thin layer (Gadelha et al., 2007; Holwill and McGregor, 1975; Wheeler, 2017). Evidence for planarity – that the whole flagellum appears in focus when the beat and focal planes are parallel – is also qualitative and limited by microscope z resolution. To address this, *L. mexicana* promastigotes expressing mNeonGreen (mNG) fused to the flagellum membrane protein SMP1 were analysed by multifocal plane microscopy, focusing away from the coverslip to avoid surface effects. A 200 Hz frame rate could be achieved, with <1 photon/px background and signal up to 15 photons/px (Fig. 3A,B; Movie 3A,B).

Most *Leishmania* underwent a tip-to-base symmetrical flagellar beat with the beat plane oriented randomly relative to the focal planes. A few cells rotated sufficiently quickly that, within a single video (4.75 s), their beat plane rotated from near-parallel to near-perpendicular, giving orthogonal views of a single cell (Fig. 3C,D). The 3D flagellum conformation was reconstructed by recording where it intersected with a focal plane while beating near-perpendicular to the focal planes (Fig. 3E–M). By considering a cell that rotates over the video, the beat reconstruction from
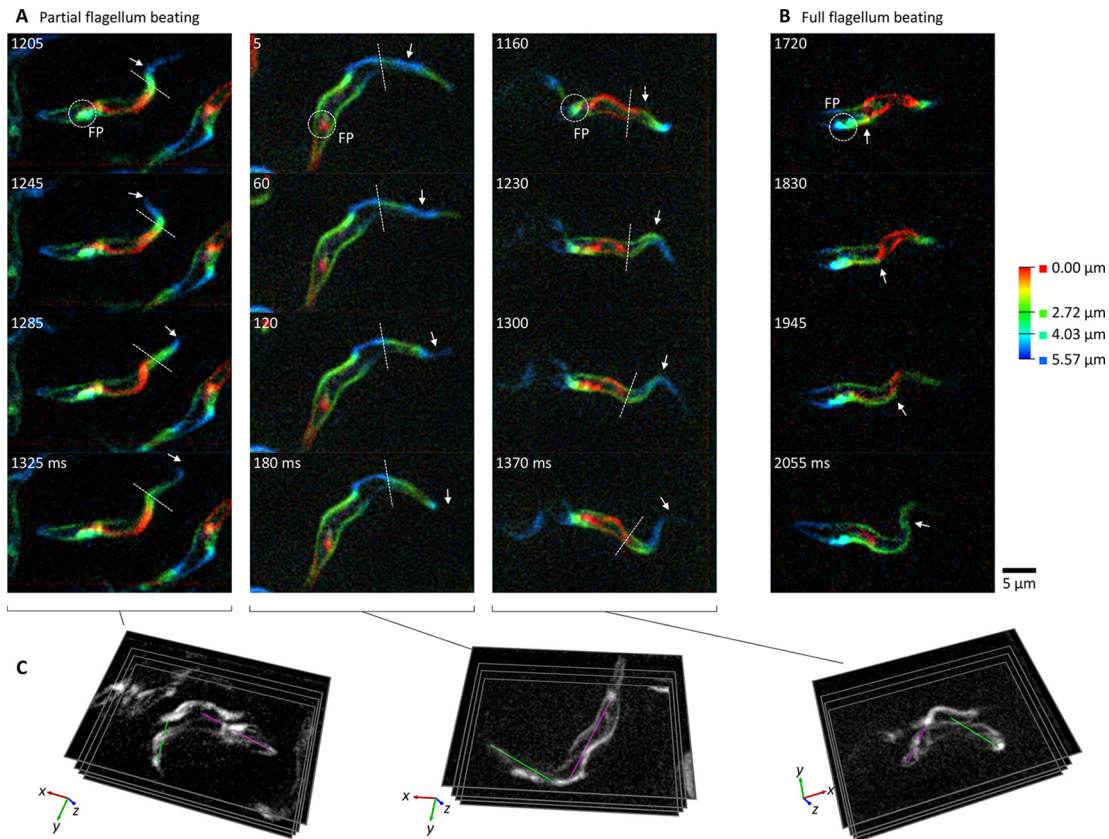
Fig. 2. The distal flagellum beat reverses while the proximal flagellum curves the cell in tumbling *T. brucei*. All panels show frames from 200 Hz multifocal plane videos of procyclic forms labelled with FM 4-64FX (Movie 2). (A) Three examples of typical tumbling cell movement showing four frames covering one beat at ~5 Hz. FP indicates the flagellar pocket, arrows indicate a propagating wavefront, dotted lines indicate the boundary between the beating and 'locked' flagellum portions. (B) One example of the less common flagellum movement in tumbling cells where waves propagate along the entire flagellum. (C) 3D conformation of the cells in A highlighting the orientation of the cell anterior (green line) or posterior (magenta line) of the locked portion of the flagellum, which lie approximately perpendicular.

multifocal plane imaging can be compared to widefield imaging once it has rotated parallel to the focal plane (Fig. 3F,I,L). This confirmed accurate 3D reconstructions.

The points of flagellum–focal plane intersection can be precisely measured as the computational sub-image alignment has a small error (Fig. S1D). Flagellum beat planarity was quantified from frames where the flagellum crossed the focal planes at ≥5 points. These were fitted to a plane and planarity inferred from the residuals – the distance of points from the fitted plane. Overall, residuals were small (n=23 reconstructions from nine cells), indicating that the flagellum in any single frame was very close to planar. The mean residual (overall deviation from the plane) was 0.076±0.058 µm, while the maximum residual (maximum deviation from planarity at any single point) was also small at 0.32±0.24 µm. However, while the flagellum configuration was near-planar in individual frames, this plane oscillated over a beat cycle, particularly for short flagella (illustrated in Fig. 3C,D).

Subtle flagellum beat deviations from planar in sperm is important for cell swimming (Bukatin et al., 2015), therefore *Leishmania* deviation from planarity is probably important, perhaps for their characteristic helical swimming paths (Wheeler, 2017). *Leishmania* experience a force- and torque-free low Reynolds number environment, therefore there must be an asymmetric cell body motion to allow flagellum beat plane rotation. This implicates the flagellum–cell body interface as giving rise to variation in the beat plane, perhaps proximal flagellum-specific outer dynein arm complexes (Edwards et al., 2018) or alternatively, flagellum

anchoring in the flagellar pocket by the flagellum attachment zone (Wheeler et al., 2016).

Conclusions

This work demonstrates that multifocal plane fluorescence microscopy is capable of analysing volumes and frame rates useful for interrogating flagellum beating using either chemical or native fluorescent protein fluorescence. This is, to our knowledge, the highest frame rate biological application of this approach and the first 3D reconstruction of flagellum beating using fluorescence. Analysis of *T. brucei* tumbling and *L. mexicana* forward swimming approach highlighted how small changes in cell movement or configuration (a curved cell shape in *T. brucei* or a varying beat plane in *L. mexicana*) alter cell swimming, which may be important for collective motility or chemotaxis. It also further emphasised how the coupling of flagellum movement to the cell body by the flagellum attachment zone and how proximal and/or distal differences in the outer dynein arms may regulate trypanosomatid swimming.

The approach demonstrated here is transferrable to other species or ciliated and flagellated tissue, and specificity of fluorescence labelling provides key advantages over transmitted light used in digital holography and bright-field defocus methods. There are also more complex applications, for example a labelled cell crowded by unlabelled tissue or other cells – in trypanosomes such conditions are where collective motility occurs. Labelling of a specific cellular substructure is also powerful, particularly for complex multi-flagellated cells like *Giardia* and *Trichomonas*. High-speed
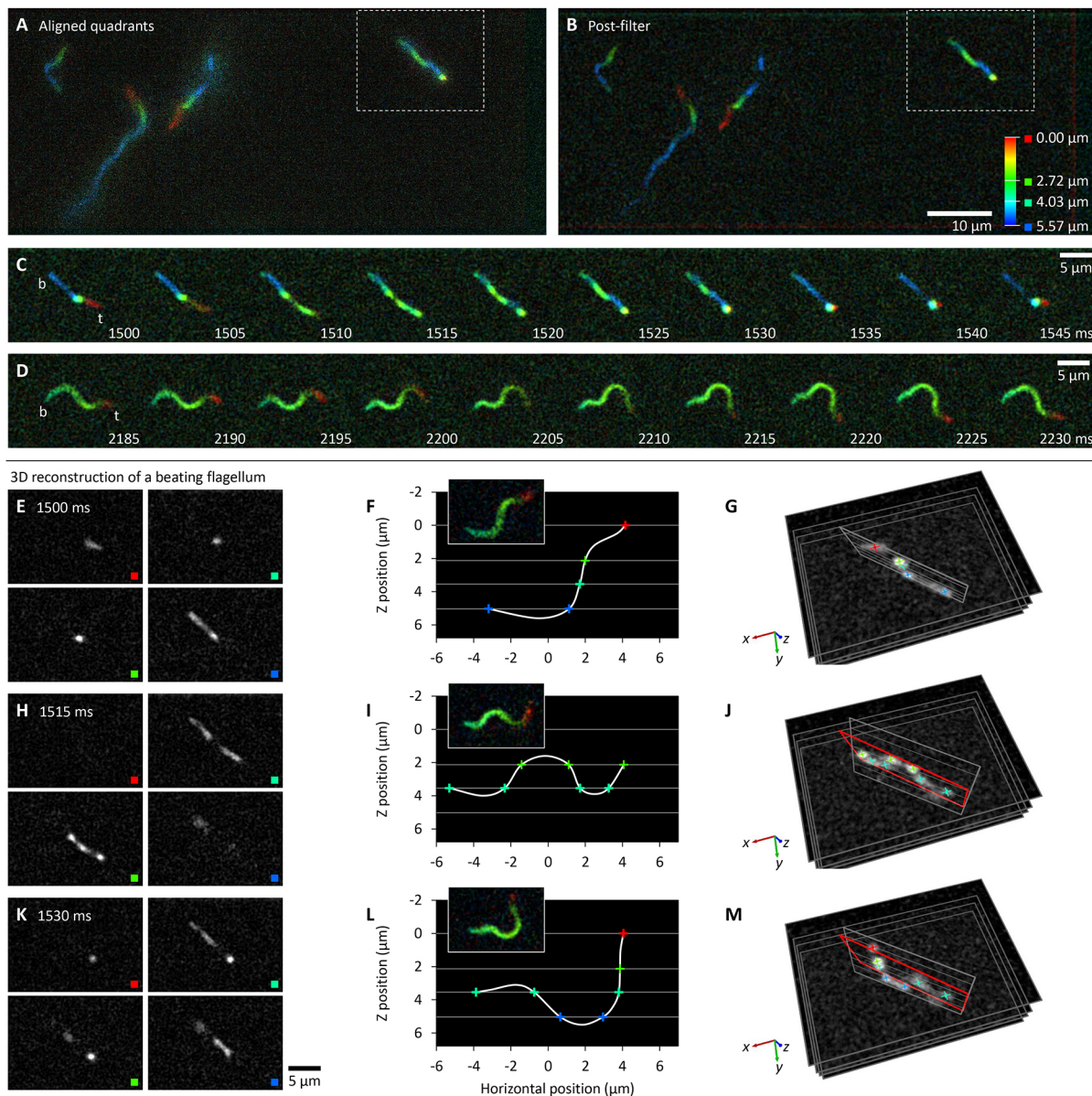
Fig. 3. The _L. mexicana_ flagellar beat does not remain in a single plane. All panels show frames from a 200 Hz multifocal plane video of promastigotes expressing SMP1::mNG (Movie 3). (A) One example frame, following sub-image alignment and pseudocolouring according to focal depth. (B) The image in A following filtering. (C,D) Movement of an example flagellum, outlined by white box in A and B, beating at ~20 Hz. Labels indicate the flagellum base (b) and tip (t). (C) One beat when the beat and focal planes are perpendicular. (D) One beat from the same cell, 0.7 s later, when the beat and focal planes are parallel. (E–M) 3D flagellum conformation from three frames (1500 ms, 1515 ms and 1530 ms in C). E,H,K show individual focal planes. F,I,L show plotted points of intersection of the flagellum with each focal plane. Inset, a rotated copy of 2185 ms, 2200 ms and 2215 ms, respectively, in D for comparison. (G,J,M). Direct visualisation in 3D, with J and M showing the plane in G in red.

multifocal plane microscopy is therefore a powerful approach for understanding flagellum- and/or cilium-driven dynamics.

MATERIALS AND METHODS

SmOxP9 procyclic _T. brucei_ (Poon et al., 2012) were grown in SDM79 medium (Life Technologies) with 10% FCS. Cas9T7 promastigote _L. mexicana_ (Beneke et al., 2017) were grown in M199 medium (Life Technologies) supplemented with 2.2 g/l $NaHCO_3$, 0.005% hemin, 40 mM HEPES-HCl (pH 7.4), and 10% FCS. _L. mexicana_ SMP1 (LmxM.20.1310) (Tull et al., 2004) was C-terminally tagged with mNG (Shaner et al., 2013) at the endogenous locus as previously described (Beneke et al., 2017). _T. brucei_ and _L. mexicana_ were grown at 28°C and imaged during logarithmic growth (0.5×10^7–1.0×10^7 cells/ml).

Videos were captured using a 100× NA 1.4 objective (without phase ring, Zeiss) on an Axio observer A1 (Zeiss) microscope with incubator chamber,

using a 120 V metal halide light source (Zeiss, HXP 120 V) and either an mRFP (Zeiss, 63HE) or GFP (ThorLabs, MDF-GFP2) filter cube. A MultiSplit v2 (Cairn Research) was used for multifocal plane imaging with three 50% semi-silvered mirrors in the filter cubes and a 2000 mm, 1300 mm, 500 mm or no lens in the auxiliary filter/lens mount immediately following the filter cube.

Images for calibration of focus offset, position offset and scale/ magnification aberration of each sub-image were captured using multi-wavelength fluorescent beads (TetraSpeck, Invitrogen T7279). Focus offset was measured from the relative _z_ position to focus the beads in each sub-image. Sub-image position offset and scale aberration were determined from bead pairs (one central and one peripheral bead within each sub-image) using Gaussian fitting to determine bead locations with sub-pixel accuracy.

Cells were held in a sealed 250 μm deep (deep relative to cell size) sample chamber (Gene Frame, Thermo Fisher Scientific, AB0576) between a plain

glass slide and coverslip in normal growth medium and analysed at 28°C. For FM 4-64FX (Thermo Fisher Scientific Molecular Probes, F34653) labelling at 1:100, 40 μM of the stain was included in the medium.

Videos at a length of 4750 ms at 200 Hz frame rate (5 ms/frame) were captured using a Neo 5.5 camera (Andor), vertically cropped to 50% (1080 px) around the camera midline. Constant readout column and pixel noise were subtracted (mean signal from 600 frames captured with no illumination) and random amplifier noise per row of pixels was subtracted (the median signal per pixel row per frame). Focus stacks were then generated using the necessary offset and scale corrections. Image filtering for analysis was a 2 px Gaussian blur then a 10 px rolling ball background subtraction. Image processing was performed in ImageJ (Collins, 2007).

Cell swimming was simulated using a boundary element computational framework (Pozrikidis, 2002) of a neutrally buoyant mesh approximating a procyclic *T. brucei* cell shape, essentially as previously described for *Leishmania* simulation (Walker et al., 2018; Walker et al., 2019). The *T. brucei* cell mesh was approximated from three joined tapering cylinder sections and capped with hemispheres. From anterior to posterior, written in the form (distance from anterior, diameter), cell shape was parameterised as: (0 μm, 1 μm), (6 μm, 3 μm), (12 μm, 2 μm), (18 μm, 0.5 μm). The flagellum beat was simulated as a base-to-tip sinusoid with amplitude 1.5 μm in the cell anterior (12–18 μm) and cell curvature was approximated as a circular arc in the cell mid-section (6–12 μm) to achieve a 0°, 45° or 90° cell bend.

Supplementary information
Supplementary information available online at
http://jcs.biologists.org/lookup/doi/10.1242/jcs.231795.supplemental

References
Ballesteros-Rodea, G., Santillán, M., Martínez-Calvillo, S. and Manning-Cela, R. (2012). Flagellar motility of trypanosoma cruzi epimastigotes. *J. Biomed. Biotechnol.* **2012**, 520380. doi:10.1155/2012/520380

Bargul, J. L., Jung, J., McOdimba, F. A., Omogo, C. O., Adung'a, V. O., Krüger, T., Masiga, D. K. and Engstler, M. (2016). Species-specific adaptations of trypanosome morphology and motility to the mammalian host. *PLoS Pathog.* **12**, e1005448. doi:10.1371/journal.ppat.1005448

Baron, D. M., Kabututu, Z. P. and Hill, K. L. (2007). Stuck in reverse: loss of LC1 in Trypanosoma brucei disrupts outer dynein arms and leads to reverse flagellar beat and backward movement. *J. Cell Sci.* **120**, 1513-1520. doi:10.1242/jcs.004846

Beneke, T., Madden, R., Makin, L., Valli, J., Sunter, J. and Gluenz, E. (2017). A CRISPR Cas9 high-throughput genome editing toolkit for kinetoplastids. *Open Sci.* **4**, 170095. doi:10.1098/rsos.170095

Beneke, T., Demay, F., Hookway, E., Ashman, N., Jeffery, H., Smith, J., Valli, J., Becvar, T., Myskova, J., Lestinova, T. et al. (2019). Genetic dissection of a Leishmania flagellar proteome demonstrates requirement for directional motility in sand fly infections. *PLoS Pathog.* **15**, e1007828. doi:10.1371/journal.ppat.1007828

Branche, C., Kohl, L., Toutirais, G., Buisson, J., Cosson, J. and Bastin, P. (2006). Conserved and specific functions of axoneme components in trypanosome motility. *J. Cell Sci.* **119**, 3443-3455. doi:10.1242/jcs.03078

Broadhead, R., Dawe, H. R., Farr, H., Griffiths, S., Hart, S. R., Portman, N., Shaw, M. K., Ginger, M. L., Gaskell, S. J., McKean, P. G. et al. (2006). Flagellar motility is required for the viability of the bloodstream trypanosome. *Nature* **440**, 224-227. doi:10.1038/nature04541

Bukatin, A., Kukhtevich, I., Stoop, N., Dunkel, J. and Kantsler, V. (2015). Bimodal rheotactic behavior reflects flagellar beat asymmetry in human sperm cells. *Proc. Natl. Acad. Sci. USA* **112**, 15904-15909. doi:10.1073/pnas.1515159112

Capewell, P., Cren-Travaillé, C., Marchesi, F., Johnston, P., Clucas, C., Benson, R. A., Gorman, T.-A., Calvo-Alvarez, E., Crouzols, A., Jouvion, G. et al. (2016). The skin is a significant but overlooked anatomical reservoir for vector-borne African trypanosomes. *eLife* **5**, e17716. doi:10.7554/eLife.17716

Cheung, J. L. Y., Wand, N. V., Ooi, C.-P., Ridewood, S., Wheeler, R. J. and Rudenko, G. (2016). Blocking synthesis of the variant surface glycoprotein coat in Trypanosoma brucei leads to an increase in macrophage phagocytosis due to reduced clearance of surface coat antibodies. *PLoS Pathog.* **12**, e1006023. doi:10.1371/journal.ppat.1006023

Collins, T. J. (2007). ImageJ for microscopy. *BioTechniques* **43**, 25-30. doi:10.2144/000112517

Daloglu, M. U., Luo, W., Shabbir, F., Lin, F., Kim, K., Lee, I., Jiang, J.-Q., Cai, W.-J., Ramesh, V., Yu, M.-Y. et al. (2018). Label-free 3D computational imaging of spermatozoon locomotion, head spin and flagellum beating over a large volume. *Light Sci. Appl.* **7**, 17121. doi:10.1038/lsa.2017.121

Edwards, B. F. L., Wheeler, R. J., Barker, A. R., Moreira-Leite, F. F., Gull, K. and Sunter, J. D. (2018). Direction of flagellum beat propagation is controlled by proximal/distal outer dynein arm asymmetry. *Proc. Natl. Acad. Sci. USA* **115**, E7341-E7350. doi:10.1073/pnas.1805827115

Eliaz, D., Kannan, S., Shaked, H., Arvatz, G., Tkacz, I. D., Binder, L., Waldman Ben-Asher, H., Okalang, U., Chikne, V., Cohen-Chalamish, S. et al. (2017). Exosome secretion affects social motility in Trypanosoma brucei. *PLoS Pathog.* **13**, e1006245. doi:10.1371/journal.ppat.1006245

Engstler, M., Pfohl, T., Herminghaus, S., Boshart, M., Wiegertjes, G., Heddergott, N. and Overath, P. (2007). Hydrodynamic flow-mediated protein sorting on the cell surface of trypanosomes. *Cell* **131**, 505-515. doi:10.1016/j.cell.2007.08.046

Forestier, C.-L., Machu, C., Loussert, C., Pescher, P. and Späth, G. F. (2011). Imaging host cell-Leishmania interaction dynamics implicates parasite motility, lysosome recruitment, and host cell wounding in the infection process. *Cell Host Microbe* **9**, 319-330. doi:10.1016/j.chom.2011.03.011

Gadelha, C., Wickstead, B. and Gull, K. (2007). Flagellar and ciliary beating in trypanosome motility. *Cell Motil. Cytoskelet.* **64**, 629-643. doi:10.1002/cm.20210

Gan, Z., Ram, S., Ober, R. J. and Ward, E. S. (2013). Using multifocal plane microscopy to reveal novel trafficking processes in the recycling pathway. *J. Cell Sci.* **126**, 1176-1188. doi:10.1242/jcs.116327

Heddergott, N., Krüger, T., Babu, S. B., Wei, A., Stellamanns, E., Uppaluri, S., Pfohl, T., Stark, H. and Engstler, M. (2012). Trypanosome motion represents an adaptation to the crowded environment of the vertebrate bloodstream. *PLoS Pathog.* **8**, e1003023. doi:10.1371/journal.ppat.1003023

Hoare, C. A. and Wallace, F. G. (1966). Developmental stages of trypanosomatid flagellates: a new terminology. *Nature* **212**, 1385-1386. doi:10.1038/2121385a0

Holwill, M. E. J. (1965). The motion of strigomonas oncopelti. *J. Exp. Biol.* **42**, 125-137.

Holwill, M. E. J. and McGregor, J. L. (1975). Control of flagellar wave movement in Crithidia oncopelti. *Nature* **255**, 157-158. doi:10.1038/255157a0

Imhof, S. and Roditi, I. (2015). The social life of African trypanosomes. *Trends Parasitol.* **31**, 490-498. doi:10.1016/j.pt.2015.06.012

Krüger, T., Schuster, S. and Engstler, M. (2018). Beyond blood: African trypanosomes on the move. *Trends Parasitol.* **34**, 1056-1067. doi:10.1016/j.pt.2018.08.002

Oberholzer, M., Lopez, M. A., McLelland, B. T. and Hill, K. L. (2010). Social motility in African trypanosomes. *PLoS Pathog.* **6**, e1000739. doi:10.1371/journal.ppat.1000739

Poon, S. K., Peacock, L., Gibson, W., Gull, K. and Kelly, S. (2012). A modular and optimized single marker system for generating Trypanosoma brucei cell lines expressing T7 RNA polymerase and the tetracycline repressor. *Open Biol.* **2**, 110037. doi:10.1098/rsob.110037

Pozrikidis, C. (2002). *A Practical Guide to Boundary Element Methods with the Software Library BEMLIB*. Boca Raton, FL, USA: CRC Press.

Prabhat, P., Gan, Z., Chao, J., Ram, S., Vaccaro, C., Gibbons, S., Ober, R. J. and Ward, E. S. (2007). Elucidation of intracellular recycling pathways leading to exocytosis of the Fc receptor, FcRn, by using multifocal plane microscopy. *Proc. Natl. Acad. Sci. USA* **104**, 5889-5894. doi:10.1073/pnas.0700337104

Purcell, E. M. (1977). Life at low Reynolds number. *Am. J. Phys.* **45**, 3-11. doi:10.1119/1.10903

Rodríguez, J. A., Lopez, M. A., Thayer, M. C., Zhao, Y., Oberholzer, M., Chang, D. D., Kisalu, N. K., Penichet, M. L., Helguera, G., Bruinsma, R. et al. (2009). Propulsion of African trypanosomes is driven by bihelical waves with alternating chirality separated by kinks. *Proc. Natl. Acad. Sci. USA* **106**, 19322-19327. doi:10.1073/pnas.0907001106

Rotureau, B., Ooi, C.-P., Huet, D., Perrot, S. and Bastin, P. (2013). Forward motility is essential for trypanosome infection in the tsetse fly. *Cell. Microbiol.* **16**, 425-433. doi:10.1111/cmi.12230

Saada, E. A., DeMarco, S. F., Shimogawa, M. M. and Hill, K. L. (2015). "With a little help from my friends"-social motility in Trypanosoma brucei. *PLoS Pathog.* **11**, e1005272. doi:10.1371/journal.ppat.1005272

Schuster, S., Krüger, T., Subota, I., Thusek, S., Rotureau, B., Beilhack, A. and Engstler, M. (2017). Developmental adaptations of trypanosome motility to the

tsetse fly host environments unravel a multifaceted in vivo microswimmer system. *eLife* **6**, e27656. doi:10.7554/eLife.27656

Shaner, N. C., Lambert, G. G., Chammas, A., Ni, Y., Cranfill, P. J., Baird, M. A., Sell, B. R., Allen, J. R., Day, R. N., Israelsson, M. et al. (2013). A bright monomeric green fluorescent protein derived from Branchiostoma lanceolatum. *Nat. Methods* **10**, 407-409. doi:10.1038/nmeth.2413

Shimogawa, M. M., Ray, S. S., Kisalu, N., Zhang, Y., Geng, Q., Ozcan, A. and Hill, K. L. (2018). Parasite motility is critical for virulence of African trypanosomes. *Sci. Rep.* **8**, 9122. doi:10.1038/s41598-018-27228-0

Silva-Villalobos, F., Pimentel, J. A., Darszon, A. and Corkidi, G. (2014). Imaging of the 3D dynamics of flagellar beating in human sperm. In 2014 36th Annual International Conference of the IEEE Engineering in Medicine and Biology Society, pp. 190-193. doi:10.1109/EMBC.2014.6943561

Subota, I., Julkowska, D., Vincensini, L., Reeg, N., Buisson, J., Blisnick, T., Huet, D., Perrot, S., Santi-Rocca, J., Duchateau, M. et al. (2014). Proteomic analysis of intact flagella of procyclic Trypanosoma brucei cells identifies novel flagellar proteins with unique sub-localization and dynamics. *Mol. Cell. Proteomics* **13**, 1769-1786. doi:10.1074/mcp.M113.033357

Sun, S. Y., Kaelber, J. T., Chen, M., Dong, X., Nematbakhsh, Y., Shi, J., Dougherty, M., Lim, C. T., Schmid, M. F., Chiu, W. et al. (2018). Flagellum couples cell shape to motility in Trypanosoma brucei. *Proc. Natl. Acad. Sci. USA* **115**, E5916-E5925. doi:10.1073/pnas.1722618115

Trindade, S., Rijo-Ferreira, F., Carvalho, T., Pinto-Neves, D., Guegan, F., Aresta-Branco, F., Bento, F., Young, S. A., Pinto, A., Van Den Abbeele, J. et al. (2016). Trypanosoma brucei parasites occupy and functionally adapt to the adipose tissue in mice. *Cell Host Microbe* **19**, 837-848. doi:10.1016/j.chom.2016.05.002

Tull, D., Vince, J. E., Callaghan, J. M., Naderer, T., Spurck, T., McFadden, G. I., Currie, G., Ferguson, K., Bacic, A. and McConville, M. J. (2004). SMP-1, a member of a new family of small myristoylated proteins in kinetoplastid parasites, is targeted to the flagellum membrane in Leishmania. *Mol. Biol. Cell* **15**, 4775-4786. doi:10.1091/mbc.e04-06-0457

Uppaluri, S., Nagler, J., Stellamanns, E., Heddergott, N., Herminghaus, S., Engstler, M. and Pfohl, T. (2011). Impact of microscopic motility on the swimming behavior of parasites: straighter trypanosomes are more directional. *PLoS Comput. Biol.* **7**, e1002058. doi:10.1371/journal.pcbi.1002058

Walker, P. J. (1961). Organization of function in trypanosome flagella. *Nature* **189**, 1017-1018. doi:10.1038/1891017a0

Walker, B. J., Ishimoto, K., Wheeler, R. J. and Gaffney, E. A. (2018). Response of monoflagellate pullers to a shearing flow: a simulation study of microswimmer guidance. *Phys. Rev. E* **98**, 063111. doi:10.1103/PhysRevE.98.063111

Walker, B. J., Wheeler, R. J., Ishimoto, K. and Gaffney, E. A. (2019). Boundary behaviours of Leishmania mexicana: a hydrodynamic simulation study. *J. Theor. Biol.* **462**, 311-320. doi:10.1016/j.jtbi.2018.11.016

Wheeler, R. J. (2017). Use of chiral cell shape to ensure highly directional swimming in trypanosomes. *PLoS Comput. Biol.* **13**, e1005353. doi:10.1371/journal.pcbi.1005353

Wheeler, R. J., Sunter, J. D. and Gull, K. (2016). Flagellar pocket restructuring through the Leishmania life cycle involves a discrete flagellum attachment zone. *J. Cell Sci.* **129**, 854-867. doi:10.1242/jcs.183152

Wilson, L. G., Carter, L. M. and Reece, S. E. (2013). High-speed holographic microscopy of malaria parasites reveals ambidextrous flagellar waveforms. *Proc. Natl. Acad. Sci. USA* **110**, 18769-18774. doi:10.1073/pnas.1309934110

Quadrant 0, z=0.00 μm ■ Quadrant 2, z=4.03 μm
Quadrant 1, z=2.72 μm ■ Quadrant 3, z=5.57 μm

10 μm
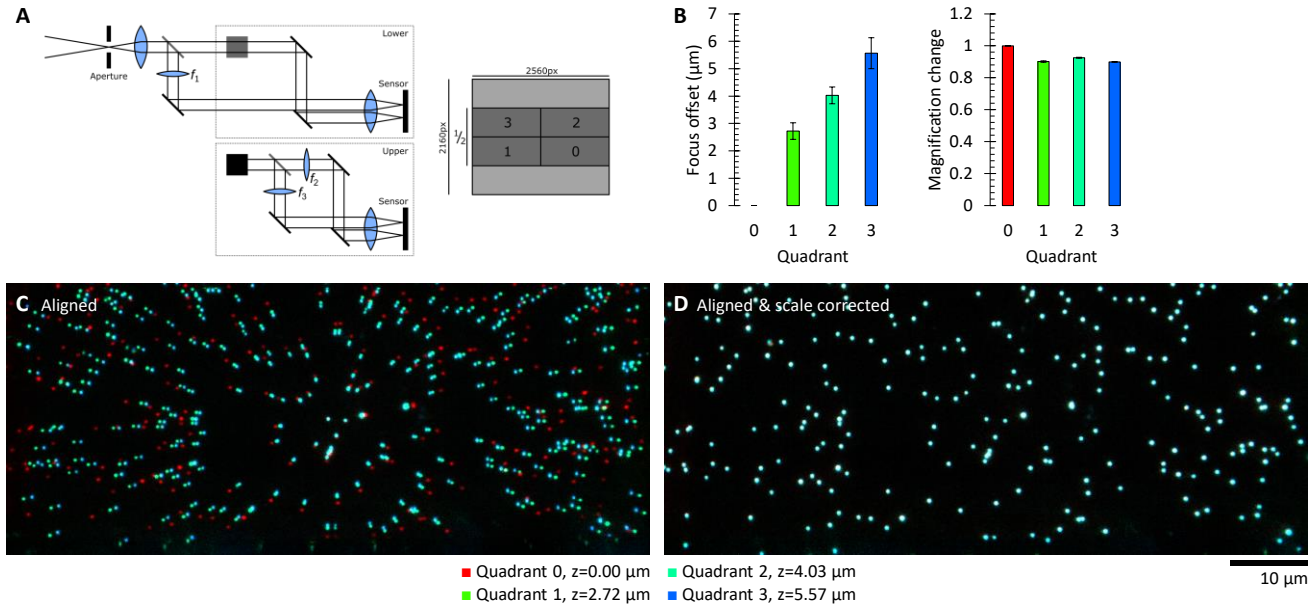
Fig. S1. Setup and calibration of the multifocal plane system. A. Overview of the light path through the multi-splitter to achieve images of the same region but with offset focal planes on four quadrants of the camera sensor. Semi-silvered mirrors are shown in grey, fully-silvered in black. The light path is 3D, with the grey square (representing a semi-silvered mirror) in the lower section reflecting light upwards, out of the plane of the page/screen, and the black square (representing a fully-silvered mirror) in the upper section reflecting it back to parallel with the page/screen. Only half (full width, vertically centred) of the camera sensor was used, allowing a 200 Hz frame rate. f_1 = 2000 mm, f_2 = 1300 mm, f_3 = 500 mm. **B.** The measured offset in focal plane for the four quadrants and the measured scale/magnification aberration for the four quadrants relative to the light path with no additional lens. Error bars represent the standard deviation, n = 5. **C.** Example of images aligned from the four quadrants (captured at the appropriate stage height for the beads to be in focus) without correction for the scale/magnification aberration. **D.** The same set of images aligned from the four quadrants with scale/magnification correction, showing precise co-localisation. Offset and scale parameters were accepted if the mean offset between points from different channels was <1 px (<65 nm).
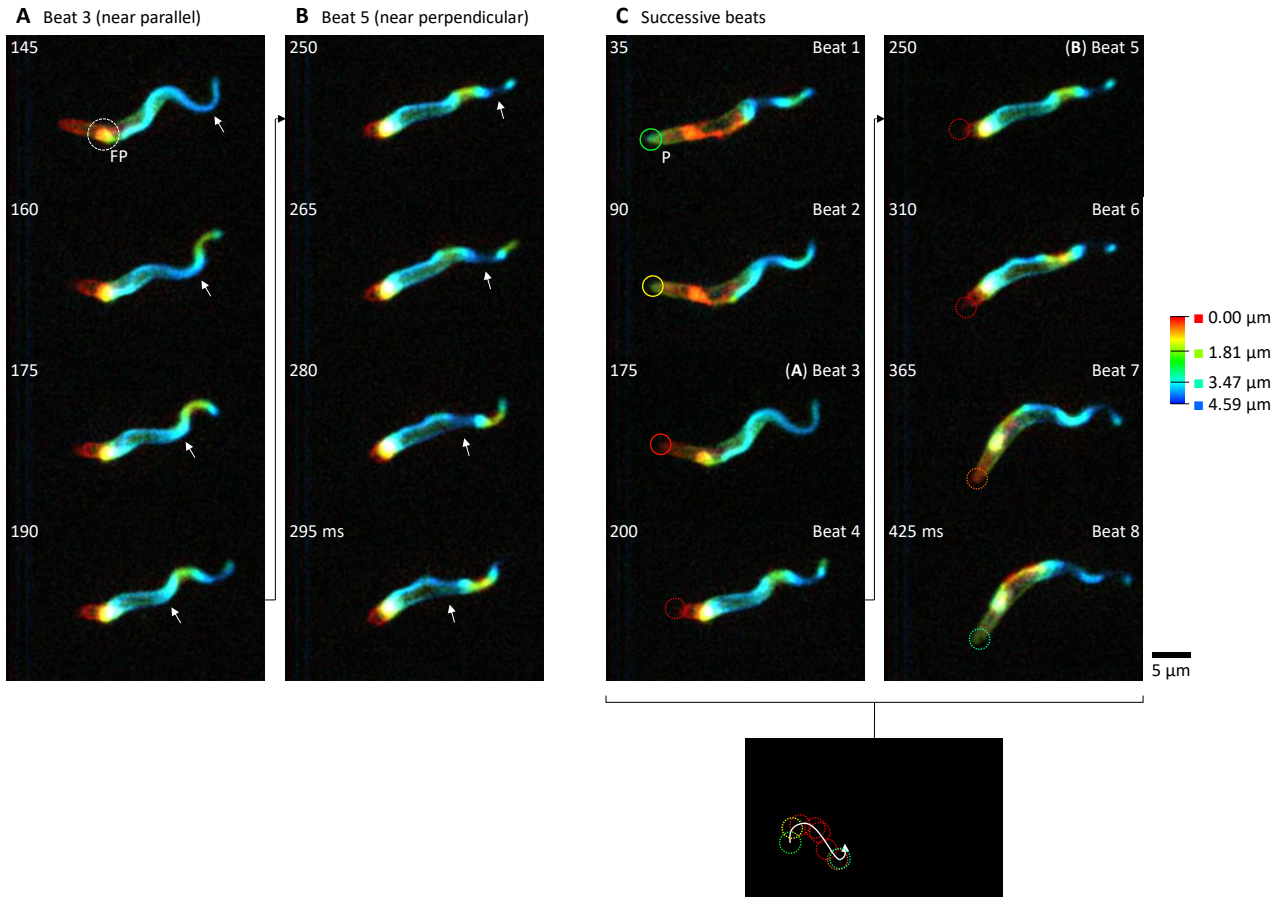
Fig. S2. Forward swimming *Trypanosoma brucei* undergo a tip-to-base whole-flagellum beat while undergoing longitudinal rotation, as previously described. All panels show frames from a 200 Hz multifocal plane videos of a *T. brucei* procyclic form labelled with a fluorescent membrane stain. **A.** Example of the flagellum movement in a forward swimming *T. brucei* procyclic cell showing four frames covering one beat cycle (beat frequency ~20 Hz) while the flagellum beat plane is near parallel to the focal planes. Waves propagate from the flagellum tip to the base along the entire flagellum. FP indicates the flagellar pocket at the base of the flagellum, arrows indicate a propagating wavefront. **B.** Four more frames of the same *T. brucei* procyclic form cell as in A showing one beat cycle where the cell has rotated such that the flagellum beat plane is near perpendicular to the focal planes. **C.** The appearance of the same *T. brucei* procyclic cell at the start of the beat cycle for 8 successive flagellar beats. P indicates the posterior of the cell, whose position as the cell swims forward is summarised at the bottom of panel C. The cell completes one longitudinal revolution over the 8 beat cycles.
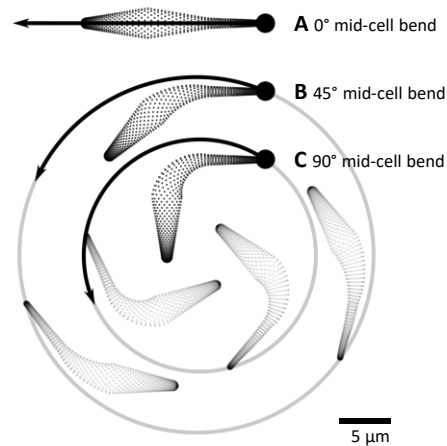
Fig. S3. Simulated paths of procyclic *T. brucei*-shaped cells driven by beating approximating observed tumbling cells. Swimming path of a mesh approximating the shape of the procyclic *T. brucei* cell moving in a low Reynolds number environment driven by a sinusoid beat in the anterior third of the cell, which approximates beating in only the distal half of the flagellum, and with different degrees of bending in the mid-cell, which approximates a locked flagellum curvature in the proximal half of the flagellum. The large circles indicate the start point of the anterior tip of the cell, the solid arrow indicates the path followed in a fixed time interval, and (for curved paths) the light grey line and ghosted cell shapes show the longer time scale behaviour. **A.** 0° bend in the mid-cell (straight cell). **B.** 45° bend in the mid-cell. **C.** 90° bend in the mid-cell, similar to the perpendicular orientation of the cell posterior and beating portion of the cell anterior observed for tumbling cells (Fig. 2).
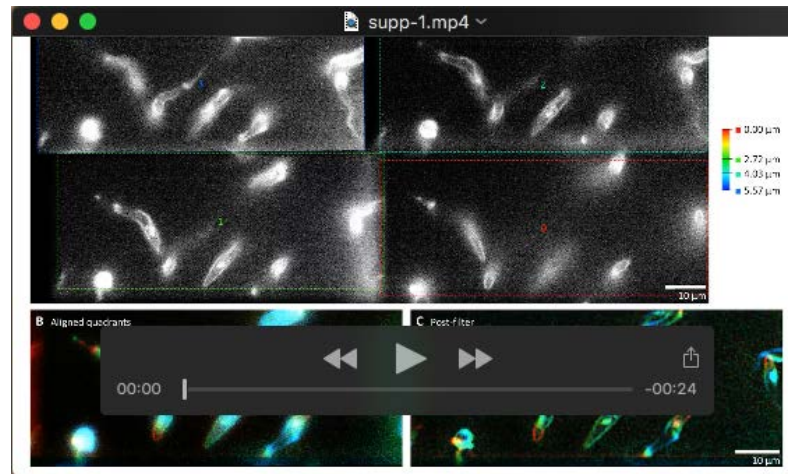
Movie 1. High-speed multifocal plane microscopy to visualise live swimming *T. brucei* in 3D. Animated version of Fig. 1, showing panels B-D. Playback is at 25 Hz frame rate (1/8 real time).
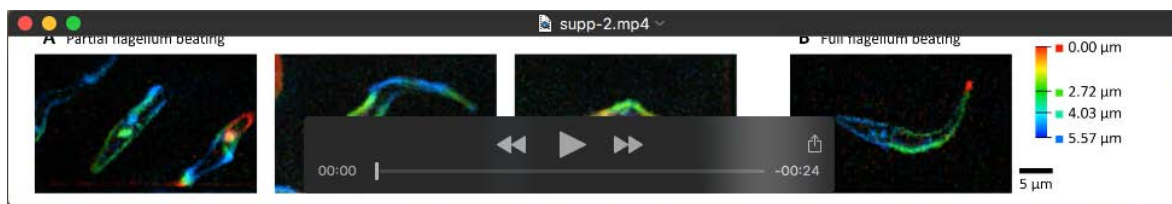
Movie 2. The distal flagellum beat reverses while the proximal flagellum curves the cell in tumbling *T. brucei*. Animated version of Fig. 2 showing panels A-B. Playback is at 25 Hz frame rate (1/8 real time).
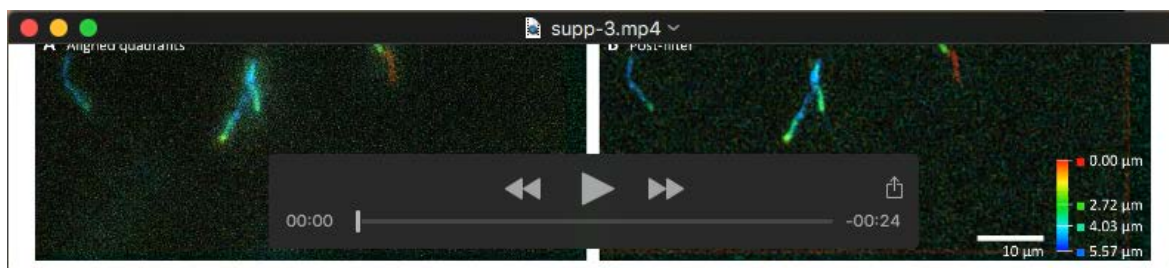
Movie 3. The *L. mexicana* flagellar beat does not remain in a single plane. Animated version of Fig. 3 showing panels A-B. Playback is at 25 Hz frame rate (1/8 real time).